IEEE Access
Multidisciplinary | Rapid Review | Open Access Journal

Received October 5, 2021, accepted November 8, 2021, date of publication December 8, 2021, date of current version December 27, 2021.

Digital Object Identifier 10.1109/ACCESS.2021.3134202

Active Vibration Control of Seismically Excited Building Structures by Upgraded Grey Wolf Optimizer

MAHDI AZIZI[1], SIAMAK TALATAHARI[1,2], AND AGATHOKLIS GIARALIS[3]

[1]Department of Civil Engineering, University of Tabriz, Tabriz 5166616471, Iran
[2]Faculty of Engineering, Near East University, 99150 Nicosia, Turkey
[3]Department of Civil Engineering, City, University of London, London EC1V 0HB, U.K.

Corresponding author: Agathoklis Giaralis (agathoklis.giaralis.1@city.ac.uk)

This work was supported by the Engineering and Physical Sciences Research Council (EPSRC), U.K., under Grant EP/M017621/1. The work of Mahdi Azizi and Siamak Talatahari was supported by the Research Grant of the Iran National Science Foundation (INSF) under Grant 99011998.

ABSTRACT In recent decades, active vibration control of buildings for earthquake-induced damage mitigation has been widely considered in the scientific literature. Model-free controllers using human knowledge-based fuzzy logic rules were shown to be advantageous over conventional model-based controllers as their effectiveness is not limited by the accuracy of the structural modelling of buildings. The latter becomes challenging in view of nonlinear building response under severe seismic excitations and uncertainties to the structural properties at the time of the seismic event. Nevertheless, the specification of fuzzy logic controllers (FLCs) relying only on expert knowledge may not result in optimal control response. At the same time, the pursue of optimizing fuzzy logic control rules based on excitation and structural response data, beyond human expert knowledge, is not straightforward as it increases considerably the scale of the optimal FLC design problem. To this end, this paper puts forth an enhanced version of the Upgraded Grey Wolf Optimizer (UGWO) to optimally design membership functions and rule bases of FLC to minimize seismic structural damage. The latter is defined in terms of maximum curvature ductility ratio at the ends of structural members. The potential of the UGWO is demonstrated by considering FLC-based optimal seismic active control in a 20-story steel benchmark structure with nonlinear behavior involving more than 400 design variables. The performance of the UGWO is gauged by examining nine different structural performance metrics and compared to results of 5 different widely used state-of-art metaheuristic optimization algorithms including the standard Grey Wolf Optimizer. Comparisons demonstrate the capability of UGWO to provide improved seismic performance, resulting in reduced structural responses and damages for the considered benchmark structure.

INDEX TERMS Ground motion, fuzzy logic controller, optimization, upgraded grey wolf optimizer, active seismic control.

I. INTRODUCTION

A. BACKGROUND AND MOTIVATION

High-rise slender buildings are increasingly dominating the skyline of modern cities, making efficient use of the ever-more scarce and high-premium urban land [1]. However, when located in high seismicity regions, these structures may be susceptible to wide-band earthquake-induced lateral loads [2]. To this end, active vibration control approaches have been widely pursued in the scientific literature for suppressing earthquake-borne lateral oscillations in high-rise buildings [3], aiming to increase community resilience to the seismic hazard. Such approaches employ large-scale actuators to exert time-varying control forces to buildings in order to reduce seismic structural demands, namely lateral relative inter-story displacements (story drifts) and floor accelerations. The required control forces are determined by closed-loop optimal feedback control algorithms, informed by real-time measurements of structural responses and ground motion excitations. Despite promising theoretical

The associate editor coordinating the review of this manuscript and approving it for publication was Giovanni Pau.

studies, active control technology found little practical application, compared to passive control solutions for the seismic protection of buildings. This is mostly due to the large external energy typically required to generate the desired control forces, the cost of equipment (i.e., sensors and actuators) and the complexity and efficiency of active controllers [4]. Nevertheless, the additive cost of active seismic control is expected to reduce in the foreseeable future with the increased availability of real-time seismic ground motion and structural response data acquisition systems [5]. Such sensing systems support earthquake early warning strategies in densely populated areas [6] as well as rapid post-earthquake structural damage detection [7] to enhance seismic resilience in smart cities. Further, the efficacy and adaptiveness of active motion control over passive control solutions has been successfully demonstrated in mitigating wind-borne oscillations in real-life tall slender buildings [8]. Given that wind excitations are most critical to the design of typical tall slender buildings [9], the catalyst for extending the applicability of active control to address seismic loads in such structures is on developing more efficient active controllers tailored to minimize seismic structural demands.

The effectiveness of conventional model-based closed-loop active motion controllers depends heavily on the accuracy of the parametric mathematical model they employ to represent the dynamically excited structure [3]. This dependency undermines the potential of such controllers for effective seismic active control of complex high-rise buildings since the properties of these structures are uncertain at the time of an earthquake and their response to severe seismic ground excitation may become nonlinear [5]. In this respect, model-free intelligent fuzzy logic controllers (FLCs) were shown to be quite advantageous for active seismic control of buildings as they can handle efficiently complex phenomena such as nonlinear structural seismic response due to material yielding [10]–[13]. Nevertheless, the effectiveness of FLCs relies on heuristic control rules specified by human expertise/intuition. In previous works considering FLCs for active seismic control of buildings [12], [13], the FLC rules were taken as fixed. That is, FLC rules were strictly human knowledge-based and were not optimized using seismic excitation and structural response data. Understandably, such a consideration increases substantially the number of design variables. This is especially true for tall buildings which commonly require several actuators and underpinning FLCs spread across different stories for effective vibration control. Nevertheless, recent advances in metaheuristic optimization algorithms allow for the efficient treatment of large-scale optimization problems with several hundreds of design variables. To this end, this paper develops an improved metaheuristic optimization algorithm for efficient optimal FLC-based seismic active control of tall buildings in which fuzzy logic control rules are optimized based on structure-specific response data, looking beyond human expert knowledge.

B. LITERATURE REVIEW

There is rich literature on the use of metaheuristic optimization algorithms for FLC design in various engineering applications, some of which are reviewed here. Reddy *et al.* [14] utilized genetic algorithms for optimal design of a nonlinear knowledge-based FLC for active control of magnetic bearings. Hein *et al.* [15] developed an interpretable FLC based on the Particle Swarm Optimization for adjusting controller parameters in vibration control of industrial facilities. Vanishree and Ramesh [16] utilized the dragonfly algorithm for optimal configuration of the Static VAR compensator developed for power transmission systems with improved voltage profile. Azizipanah-Abarghooee *et al.* [17] developed a fuzzy logic-based load frequency control technique utilizing the Jaya algorithm to reduce the oscillation of system frequency. Hasanipanah *et al.* [18] proposed a new hybrid methodology for the optimal design of fuzzy systems by the Imperialist Competitive Algorithm for ground vibration from blasting at mines. Boubertakh [19] proposed a method based on the ant colony optimization algorithm for optimal design of Fuzzy PID (FPID) controllers for single-input single-output and multiple-input multiple-output systems. Caraveo *et al.* [20] investigated a modification process for a bio-inspired algorithm formulated based on the bee behavior, called bee colony optimization, for optimal design of fuzzy controllers. Sahoo *et al.* [21] utilized the differential evolution algorithm for optimization of FPID controller for load frequency nonlinear control of interconnected power systems. Debnath *et al.* [22] determined the optimal parameter configuration of the FPID controllers utilizing the firefly algorithm with application to the derivative filter for the frequency control with thermal non-reheat type turbine of a unified power system. Gheisarnejad [23] designed a secondary controller based on fuzzy logic for two practical models implemented in load frequency control design problem and optimized by the cuckoo search algorithm. Sahoo and Panda [24] utilized the Grey Wolf Optimization (GWO) algorithm for optimal control and frequency regulation in power systems based on the parameter configuration of a FPID controller. Zadeh and Bathaee [25] discussed load frequency control procedures for interconnected power systems considering uncertainty considerations and nonlinear term based on FLC using the harmony search algorithm. Olivas *et al.* [26] utilized the gravitational search algorithm for parameter adjusting of type-2 FLC.

Meanwhile, the authors developed several metaheuristic optimization algorithms and demonstrated their enhanced efficiency over alternative algorithms in solving various engineering design optimization problems. In brief, they developed the tribe–charged system search algorithm for parameter identification of nonlinear systems with large search domains [27], the quantum-behaved developed swarm optimizer for optimal design of tall buildings [28], the fuzzy adaptive charged system search for global optimization [29], the chaos game optimization algorithm for solving

constrained engineering design problems [30], and the atomic orbital search algorithm for solving global optimization problems [31] as well as constraint engineering design problems [32].

C. CONTRIBUTIONS

Herein, the GWO, introduced by Mirjalili *et al.* [33] is utilized, for the first time in the literature, for the optimal design of fuzzy controllers with data-driven control rules to achieve active seismic motion control and damage mitigation in slender high-rise buildings. The GWO is a metaheuristic algorithm considering agents which seek the optimal global solution by mimicking the hunting behavior of a typical pack of grey wolfs. The consideration of GWO for the task is prompted by its simplicity to tackle challenging large-scale engineering optimization problems and its capability of seeking the global optimal solution in a systematic manner. Further, an improved version of GWO, termed Upgraded GWO (UGWO), is proposed in this paper to achieve enhanced seismic structural performance through improved FLC optimal design. In the UGWO, an estimation of the optimal solution in the search domain is re-evaluated after the position of a single agent has been updated within each iteration of the algorithm, as opposed to re-evaluating the optimal solution location after the position of all the agents have been updated (i.e., at the end of each iteration) used in the standard GWO. The proposed UGWO is utilized for optimal FLC design implemented in a 20-story nonlinear steel benchmark building [34] subject to several strong recorded earthquake ground motions. The capability and performance of the UGWO for the task at hand is compared with the standard GWO alongside the latest versions of several alternative metaheuristic optimization algorithms.

II. FUZZY LOGIC CONTROLLER

A typical FLC undertakes three distinct operations. First, the FLC transcripts the input crisp data into a number of predefined linguistic arguments (fuzzy variables). This transcription operation, termed fuzzification, is based on membership functions which map input crisp data onto the fuzzy variables following fuzzy set theory. Second, an inference operation is conducted to determine the control action in the fuzzy domain. The latter operation uses a rule base of ''if-then'' fuzzy logic operators, commonly specified through human expert knowledge. Third, transcription of the control action from fuzzy variables to crisp control force values takes place, termed defuzzification. The latter operation is based on membership functions, different from those used in the fuzzification operation, mapping the fuzzy control action variables onto output crisp values. A schematic view of a FLC implemented in a closed-loop control system is presented in Fig. 1 showing the sequence of the three above-described operations: fuzzification, inference and defuzzification.

In this work, a particular FLC is adopted to regulate output active control forces for earthquake response mitigation of a building based on structural acceleration input measurements. The considered FLC is a modified version of the one proposed by Al-Dawod *et al.* [12]. The latter was strictly knowledge-based, relying on human expertise/intuition to define the support of membership functions and the rule base. For this reason, the FLC was sub-optimal and its effectiveness for structural seismic response mitigation was reported to be quite limited. Here, the FLC in [12] is modified to allow for variability to the membership function support and to the rule base, through a set of different (design) variables. Then, optimization of the design variables based on seismic structural response data allows for defining an enhanced FLC which is driven by structure-specific data rather than relying only on human knowledge.

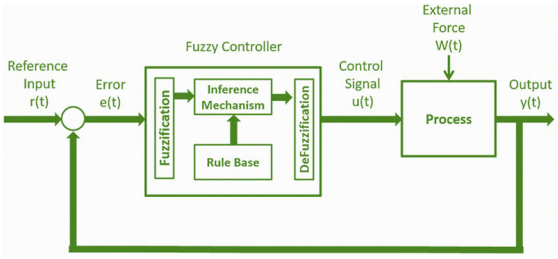

FIGURE 1. Fuzzy logic controller implemented in a closed-loop control system.

TABLE 1. Fuzzy linguistic variables.

Variables	Definition
PVL	Positive and very Large
PL	Positive and Large
PM	Positive and Medium
PS	Positive and Small
PVS	Positive and very Small
ZR	Zero
NVS	Negative and very Small
NS	Negative and Small
NM	Negative and Medium
NL	Negative and Large
NVL	Negative and very Large

In detail, the adopted FLC considers two input data streams (building response accelerations) and one output data stream (control force). Eleven linguistic fuzzy variables are utilized to define the fuzzy domain, presented in Table 1. Eight different membership functions are used for the fuzzification of each of the input data stream and eleven membership functions for the defuzzification of the output data. Membership functions are triangularly shaped with parametrically defined support through eleven variables $(a_1, a_2, \ldots, a_{11})$ for each input and fifteen variables $(b_1, b_2, \ldots, b_{15})$ for the output, as shown in Fig.2.

The rule base of the considered FLC comprises 64 ''if-then'' fuzzy rules reported in Table 2. Each rule is assigned a weight c_i $(i = 1, 2, \ldots, 64)$ taking values within [0, 1] interval, and treated as a design variable. The value of the weight c_i signifies the importance of the ith rule in the fuzzy

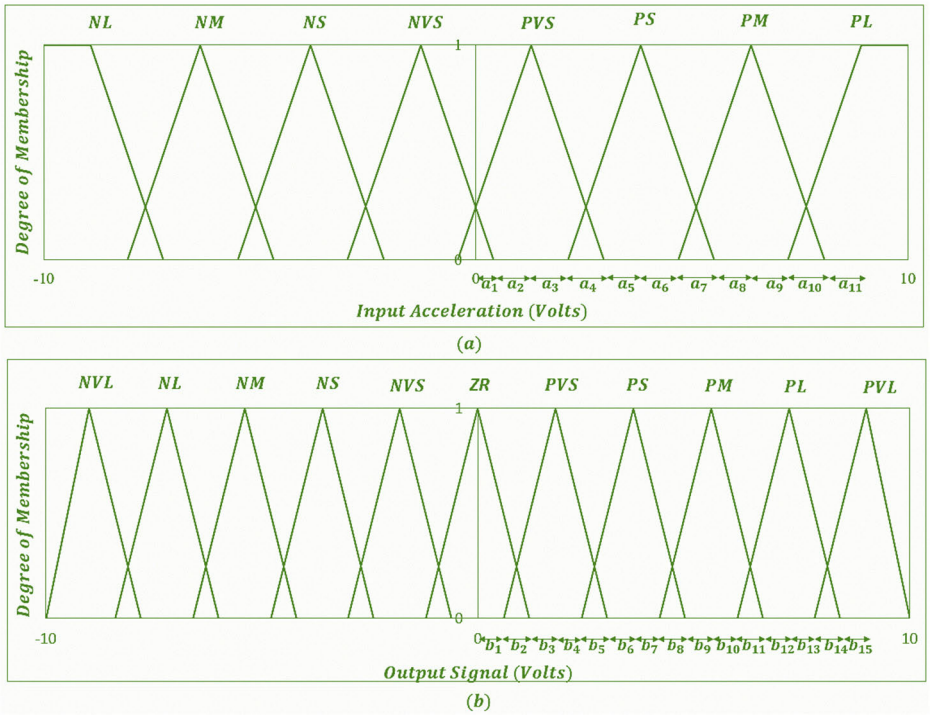

FIGURE 2. Membership functions for the input fuzzification (a) and the output defuzzification (b) with parametrically defined supports.

TABLE 2. The rule base of the FLC.

Output Control Force								
	First acceleration input							
Second acceleration input	NL	NM	NS	NVS	PVS	PS	PM	PL
NL	PVL/c1	PL/c9	PM/c17	PS/c25	PVS/c33	ZR/c41	NVS/c49	NS/c57
NM	PL/c2	PM/c10	PS/c18	PS/c26	PVS/c34	ZR/c42	NVS/c50	NS/c58
NS	PM/c3	PS/c11	PS/c19	PVS/c27	PVS/c35	ZR/c43	NVS/c51	NS/c59
NVS	PM/c4	PS/c12	PVS/c20	PVS/c28	ZR/c36	NVS/c44	NS/c52	NM/c60
PVS	PM/c5	PS/c13	PVS/c21	ZR/c29	NVS/c37	NVS/c45	NS/c53	NM/c61
PS	PS/c6	PVS/c14	ZR/c22	NVS/c30	NVS/c38	NS/c46	NS/c54	NM/c62
PM	PS/c7	PVS/c15	ZR/c23	NVS/c31	NS/c39	NS/c47	NM/c55	NL/c63
PL	PS/c8	PVS/c16	ZR/c24	NVS/c32	NS/c40	NM/c48	NL/c56	NVL/c64

rule base. For $c_i = 1$, the ith rule has maximum importance in the fuzzy inference operation, while for $c_i = 0$, the ith rule does not participate in the inference. For $0 < c_i < 1$, the ith rule has a partial participation/effect in the inference operation depending on the c_i value.

In the following section metaheuristic algorithms are reviewed to be used for optimal design of the three sets of parameters defining the adopted FLC.

III. GREY WOLF OPTIMIZER (GWO)

A. THE STANDARD GWO

The GWO is an iterative metaheuristic algorithm drawing inspiration from the hunting behavior and social hierarchy of grey wolfs to solve optimization problems, [33]. In nature, grey wolves live and hunt in a pack. During hunting, the pack first identifies some moving prey, then it encircles the prey to trap it, and ultimately attacks the prey. The GWO utilizes a predefined number of search agents whose position in the search space is iteratively updated with respect to the (unknown) position of the global optimum by mimicking the encircling behavior of individual grey wolves in a hunting pack around an identified moving pray. This behavior is mathematically modelled by firstly defining the distance between the position vector of a wolf (search agent), $\vec{X}^{(k)}$, and the position vector of pray, $\vec{X}_p{}^{(k)}$, at the kth iteration, by [33]

$$\vec{D} = \left| \vec{C}.\vec{X}_p{}^{(k)} - \vec{X}^{(k)} \right| \tag{1}$$

where

$$\vec{C} = 2\vec{r}_1 \tag{2}$$

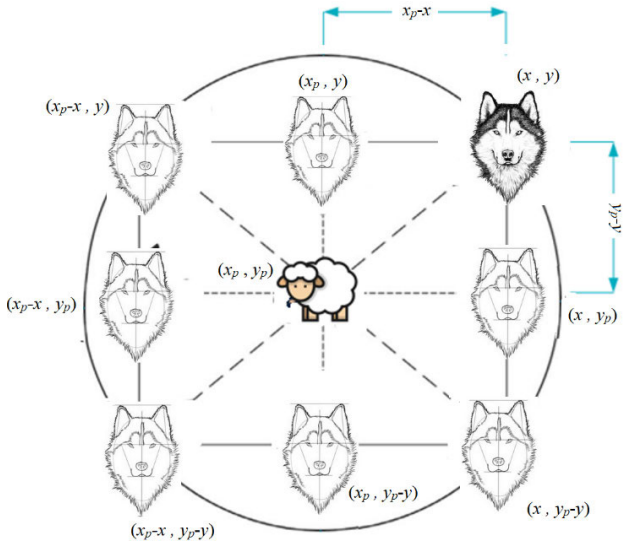

FIGURE 3. Position vectors of grey wolfs and preys in two-dimensional space.

with $\vec{r}_1$ being a vector of random numbers uniformly distributed within [0, 1]; and secondly updating the position of the wolf in the next iteration is as

$$\vec{X}^{(k+1)} = \vec{X_p}^{(k)} - \vec{A}.\vec{D} \tag{3}$$

where

$$\vec{A} = 2\vec{a}.\vec{r}_2 - \vec{a} \tag{4}$$

with $\vec{r}_2$ being a vector of random numbers uniformly distributed within [0, 1] and $\vec{a}$ being a deterministically defined vector with equal and linearly decreasing elements over the course of iterations from 2 to zero.

To facilitate a geometric interpretation of Eqs. (1-4), Fig. 3 depicts a grey wolf with current position $\vec{X}^{(k)} = (x, y)$ in a two-dimensional space and several possible updated positions around some prey located at $\vec{X_p}^{(k)} = (x_p, y_p)$. Vectors $\vec{r}_1$ and $\vec{r}_2$ allow the wolf to update its position at any point around the prey for a given vector $\vec{a}$. For example, the updated position $\vec{X}^{(k+1)} = (x_p, y_p - y)$ can be reached for $\vec{a} = (1, 1)$ by setting $\vec{r}_1 = (1, 1)$ and $\vec{r}_2 = (0.5, 1)$. Moreover, the randomness of vectors $\vec{r}_1$ and $\vec{r}_2$ whose values are different at each iteration and the monotonically reducing norm of vector $\vec{a}$ with every iteration achieve efficient coupling of and smooth transition between exploration (i.e., searching away from a local optimal solution, or prey, to find an improved solution, or better pray elsewhere) and exploitation (i.e., converging swiftly to the optimal solution once it is singled out, or attacking pray once it has been encircled), [33]. This can be appreciated by noting that for $\left|\vec{A}\right| < 1$ the updated position of the wolf will be closer to the pray and will eventually coincide for $\left|\vec{A}\right| = 0$, while for $\left|\vec{A}\right| > 1$ the wolf moves away from the pray which increases the chance of identifying alternative, potentially better, pray. Due to the randomness of $\vec{r}_2$, the value of $\left|\vec{A}\right|$ may increase or decrease in the next iteration, meaning that the search agent may "explore" moving away from a local optimal thus avoiding potential stagnation in a local solution or may "exploit" moving towards the identified solution. Importantly, the monotonic reduction of $|\vec{a}|$ in the course of iterations ensures that the probability that an agent exploits $\left(\left|\vec{A}\right| < 1\right)$ in the next iteration rather than explores $\left(\left|\vec{A}\right| > 1\right)$ increases as more iterations take place and that exploitation intensifies as $\left|\vec{A}\right|$ is more likely to take smaller values with $|\vec{a}|$ reducing in each iteration, ultimately reaching zero. Still, some level of exploration in the GWO is maintained even after several iterations through the random vector $\vec{r}_1$ or, equivalently, $\vec{C}$ which models random hurdles that a wolf may face in approaching pray. This is manifested through a stochastic increase of the distance $\vec{D}$ if $\left|\vec{C}\right| > 1$ in a subsequent iteration even though exploitation occurred (i.e., $\left(\left|\vec{A}\right| < 1\right)$) in the current iteration. Thus, vector $\vec{C}$ safeguards GWO from local optimal stagnation in the final iterations.

Further to the above considerations of randomness, exploitation, and exploration, which are important factors for all metaheuristic optimizers, the GWO benefits from a purposely unequal treatment of search agents in each iteration, reflecting the strict social ranking within any pack of grey wolves [33]. Specifically, every pack has a leader, the alpha (α) wolf who manages the pack and makes decisions, supported by a second in hierarchy deputy leader, the beta (β) wolf. Next in the hierarchy are the delta (δ) wolves who are delegated sensitive and important tasks for the pack including scouting and caretaking, and finally the lowest ranked wolves are the omega (ω) who submit to all the other dominant wolves. The GWO assumes that there is one wolf from each of the three first rankings, α, β, and δ in the hunting pack who have better knowledge of the potential location of prey and the rest are all ω wolves who update their position following the three superior wolves. Thus, at the start of the kth iteration the three obtained so-far best solutions, $\vec{X_a}^{(k)}$, $\vec{X_\beta}^{(k)}$ and $\vec{X_\delta}^{(k)}$ are selected based on the values of the objective function (fitness of solution) at the current location of all the agents and the position of all the agents are updated according to the location of the three best search agents, equally weighted. This is mathematically expressed, for the case of an arbitrary agent with position $\vec{X}^{(k)}$, by the set of equations [33]

$$\begin{cases} \vec{D_\alpha} = \left|\vec{C_1}.\vec{X_a}^{(k)} - \vec{X}^{(k)}\right| \\ \vec{D_\beta} = \left|\vec{C_2}.\vec{X_\beta}^{(k)} - \vec{X}^{(k)}\right| \\ \vec{D_\delta} = \left|\vec{C_3}.\vec{X_\delta}^{(k)} - \vec{X}^{(k)}\right| \end{cases} \tag{5}$$

$$\begin{cases} \vec{X_1} = \vec{X_a}^{(k)} - \vec{A_1}.(\vec{D_\alpha}) \\ \vec{X_2} = \vec{X_\beta}^{(k)} - \vec{A_2}.(\vec{D_\beta}) \\ \vec{X_3} = \vec{X_\delta}^{(k)} - \vec{A_3}.(\vec{D_\delta}) \end{cases} \tag{6}$$

$$\vec{X}^{(k+1)} = \frac{\vec{X_1} + \vec{X_2} + \vec{X_3}}{3} \tag{7}$$

and graphically illustrated in Fig.4.

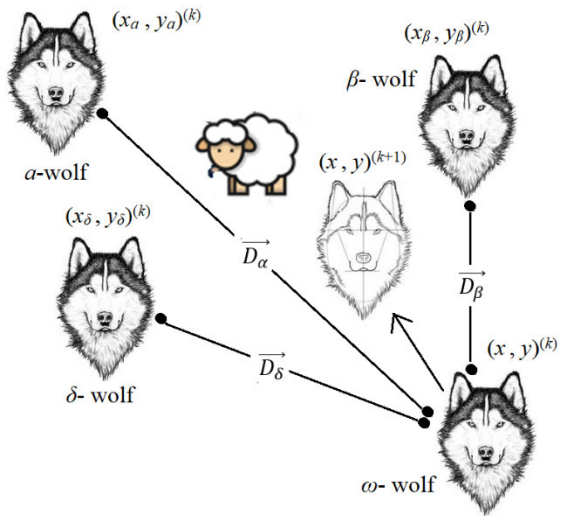

FIGURE 4. Illustration of updating the position of an ω wolf, based on the positions of the three best agents (α, β, δ wolves) with respect to the estimated position of prey in a two-dimensional space.

```
procedure Grey Wolf Optimizer (GWO)
        Initialize the grey wolf population (Xi)
        Initialize a, A and C
        Calculate the fitness of each search agent
        Evaluate Xα as the best search agent
        Evaluate Xβ as the second best search agent
        Evaluate Xδ as the third best search agent
        While t < maximum number of iterations
            for each search agent
                Update the position of the search agent by Eq. 7
            end for
            Update a, A and C
            Calculate the fitness of all search agents
            Update Xα, Xβ and Xδ
        end while
end procedure
```

FIGURE 5. Pseudo code of the GWO [33].

The pseudo code of the GWO is provided in Fig. 5, [33]. It is important to note that the use of the position of the three best agents by-passes the fact that the prey position (optimal global solution) is unknown, resulting in a feasible algorithm. It is further noted that the three best agents (dominant wolfs) may not be the same in each iteration. The latter observation motivates a proposed improvement to the GWO algorithm detailed next.

B. THE UPGRADED GREY WOLF OPTIMIZER (UGWO)

The standard GWO presented above takes a ''discrete-time'' or ''iteration-time'' approach in which the positions of the best three search agents are updated after the completion of each iteration and after the position of all agents have been updated once. Whilst the discrete-time approach for evaluating the fitness of the achieved solution is followed by most of the standard metaheuristic algorithms, the evaluation of the fitness solution within each iteration may significantly benefit the quality of final best solution in problems with large

```
procedure Upgraded Grey Wolf Optimizer (UGWO)
        Initialize the grey wolf population (Xi)
        Initialize a, A and C
        Calculate the fitness of each search agent
        Evaluate Xα as the best search agent
        Evaluate Xβ as the second best search agent
        Evaluate Xδ as the third best search agent
        While t < maximum number of iterations
            for each search agent
                Update the position of the search agent by Eq. 7
                Update a, A and C
                Calculate the fitness of all search agents
                Update Xα, Xβ and Xδ
            end for
        end while
end procedure
```

FIGURE 6. Pseudo code of the proposed UGWO.

population size. To this end, a ''continuous-time'' approached is herein utilized in which the fitness of solution is evaluated after each agent position is updated within an iteration [35]. When applied to the GWO, the continuous-time approach allows for a potential change of the three best solutions within an iteration since an ω wolf may have moved closer to pray compared to the three dominant wolves. In this setting, the UGWO is reached which enables substitution of any one of three current best solutions within an iteration once (and if) it is surpassed by an agent who just updated its position. Then, the new set of best solutions is used to update the position of the remaining agents. The modified pseudo code of the UGWO based on the continuous-time approach is presented in Fig. 6.

IV. BENCHMARK PROBLEM DESCRIPTION

A. BUILDING STRUCTURE AND NUMERICAL MODELLING

The proposed metaheuristic optimal FLC design approach is illustrated by application to a planar nonlinear computational model of a seismically excited 20-storey steel building equipped with an active control system. The structure is one of those considered in the third generation of seismic structural control benchmark problems [34]. The considered building, shown schematically in Fig.7, has been designed using a nominal design seismic action for the Los Angeles, CA, area with peak ground acceleration of 0.4g that g = 9.81m/s^2 is the gravitational constant. It is 80.77m in height and 36.58m by 30.48m in plan. It includes two underground stories with 3.65m floor-to-floor height, while the ground floor is 5.49m in height and the rest of the floors are 3.96m in height. The seismic mass of the ground and the first levels are 5.32×10^5 kg and 5.63×10^5, respectively, while for the second to 19th level, the seismic mass is 5.52×10^5 kg and for the 20th level, it is 5.84×10^5 kg.

The lateral load resisting structural system of the building comprises four perimetric steel moment resisting frames (MRFs). The purpose of the seismic active control system is to protect the MRFs along the shorter (weak) direction of the building which has 5 bays spanning 6.10m. Thus, a planar computational finite element model of one perimetric MRF,

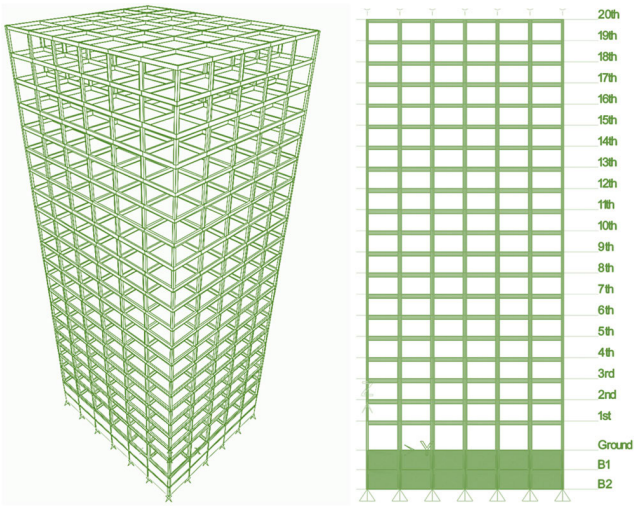

FIGURE 7. Twenty-story steel building (Left) and perimetric moment resisting frame along the weak direction (Right).

TABLE 3. Parameter specification of the nonlinear hysteresis model.

Properties	Value
Modulus of Elasticity	200,000 MPa
Yield Stress (σ_y)	345 MPa
Ultimate Stress (σ_u)	450 MPa
Yield Strain (ε_y)	0.001725
Ultimate Stain (ε_u)	0.018

shown in Fig. 7, is considered in the numerical model. Details on material and section properties for all beams and columns of the considered MRF can be found in [34].

Under severe ground shaking, the considered steel MRF is expected to behave in a nonlinear fashion [34]. This is because modern seismic design codes for ordinary buildings, such as the one used to design the structure in Fig. 7, allow for resisting seismic actions equal or above the nominal design seismic action through ductile inelastic behavior, which reduces upfront building construction costs [36]. For steel MRF buildings, this is achieved by ensuring material yielding at the ends of beams and columns with highest stress concentration resulting in the formation of flexural plastic hinges. These plastic hinges can dissipate significant input seismic (kinetic) energy without detrimental strength and stiffness degradation, thus without compromising the global structural stability. Herein, the anticipated inelastic material behavior under severe seismic action is mathematically represented by the bilinear hysteretic model in Fig. 8, utilized in subsequent nonlinear time-domain analyses. The nonlinear model properties are defined in Table 3. The standard Newmark-β implicit direct time-integration method [37] is used for nonlinear structural analysis purposes, as detailed in [38] and hard-coded in MATLAB®as detailed in [39].

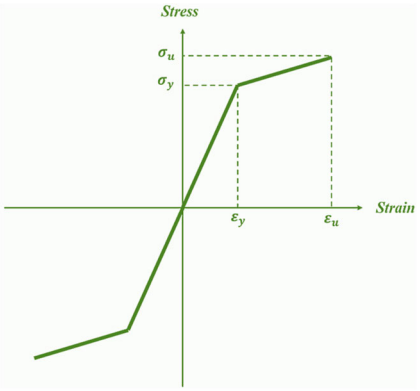

FIGURE 8. Bilinear material hysteresis model.

B. ACTIVE CONTROL SYSTEM

Whilst reducing upfront building costs, the main shortcoming of resisting severe earthquakes through nonlinear ductile material behavior is that it may incur significant monetary loss and reduced resilience in the event of major earthquakes [5]. This is because plastic hinges involve local structural damages which need to be repaired after an earthquake, alongside damages to non-structural elements, oftentimes at disproportionally high costs and downtime. To this end, the benchmark MRF is herein retrofitted by an active control system aiming to mitigate structural response to high intensity earthquakes, thus reducing the extend of nonlinear material behavior (plastic hinge formation). Following the benchmark active control problem presented in [34], active actuators are utilized to exert lateral control forces at different floors of the MRF. The maximum force capacity of each actuator is limited to 1000kN and a total of 25 actuators are provided to the MRF, with locations as seen in Fig. 9. A rigid chevron brace is used to support each actuator as shown in Fig. 9, such that an actuator placed at the n-th floor produces equal and opposite forces exerted to the n and the n + 1 floors. Five sensors acquiring lateral floor accelerations are implemented in the fourth, eighth, twelfth, sixteenth, and twentieth stories as seen in Fig. 9. Four different FLCs defined in Section II are considered to provide the required control signals to the actuators, based on data streams from the sensors. Sensors in the 4^{th} and 8^{th} stories provide input to the first FLC which governs the control forces of the actuators in the first 8 stories. Sensors in 8^{th} and 12^{th} stories provide input to a second FLC which governs the control forces of the actuators located at 9^{th} to 12^{th} stories. Sensors in 12^{th} and 16^{th} stories provide input to a third FLC which governs the control forces of the actuators located at 13^{th} to 16^{th} stories. Lastly, sensors in 16^{th} and 20^{th} stories provide input to a fourth FLC which governs control forces of the actuators located at 17^{th} to 20^{th} stories. For numerical simulation, the considered benchmark seismic active control problem is implemented in SIMULINK®as illustrated in Fig. 10.

TABLE 4. Characteristics of the selected earthquake records.

Abbr.	Earthquake - Date	Moment magnitude	Epicentral distance (km)	Fault Mechanism	Station	Component	PGA (g)
EQ1	Tabas-1978	7.4	2.05	Reverse	TABAS	TABL1	0.854
EQ2	Imperial Valley-1979	6.6	2.66	Strike Slip	Bonds Corner	BCR230	0.777
EQ3	Loma Prieta-1989	6.9	3.85	Reverse Oblique	Corralitos	CLS000	0.645
EQ4	Landers-1992	7.3	2.19	Strike Slip	Lucerne	LCN345	0.789
EQ5	Northridge-1994	6.7	5.35	Reverse	Sylmar	SCS142	0.923
EQ6	Kobe-1995	6.9	0.96	Strike Slip	KJMA	KJM000	0.834
EQ7	Chi Chi-1999	7.6	3.12	Reverse Oblique	CHY028	CHY028N	0.760

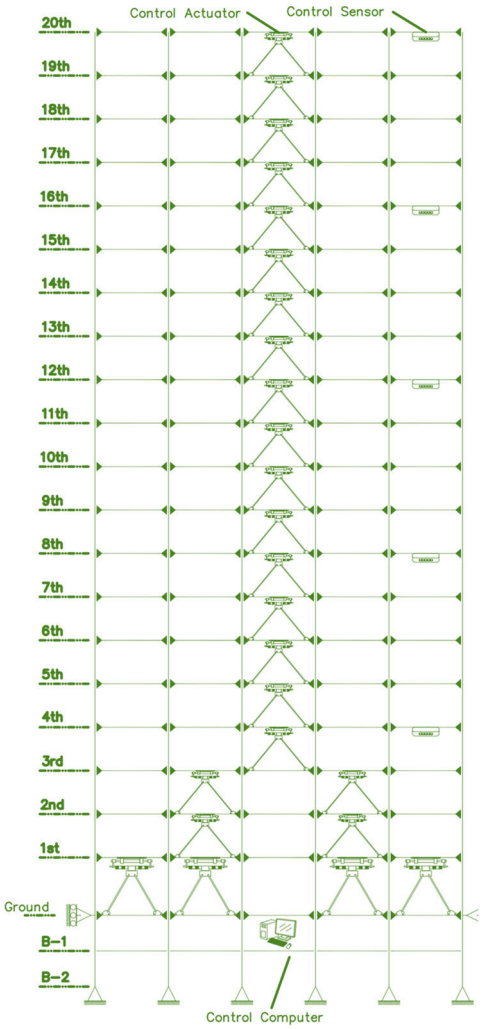

FIGURE 9. Active control system placement to the benchmark structure.

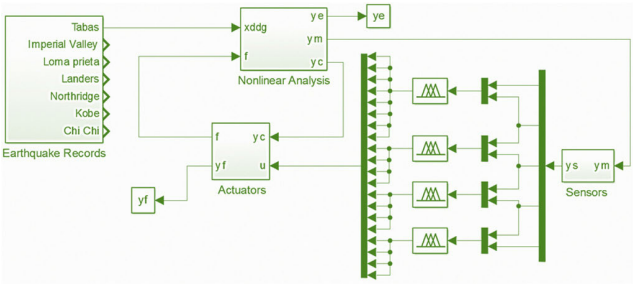

FIGURE 10. SIMULINK block diagram of the FLC-based active vibration control simulator of the 20-Story MRF building.

C. SEISMIC INPUT ACTION

In this paper, the efficacy of the benchmark active control problem shown in Fig. 9 is numerically evaluated by considering 7 acceleration ground motion signals recorded during different major historic earthquake events with moment magnitude in the range of 6.6 to 7.6. Purposely, high-intensity near-fault ground motion records are chosen with epicentral distance in the range of 0.96km to 5.35km, to incur yielding (nonlinear response) to the benchmark structure. The number of records (7) is consistent with mandates of current building codes of practice for seismic design of structures [32]. Table 4 provides details of the events along with seismological characteristics and the absolute peak ground acceleration (PGA). The latter is the most used seismic intensity measure in earthquake engineering to characterize the damage potential of strong ground motions. It is seen that the considered records have PGA $\geq$ 0.65g, which is significantly higher from the nominal design PGA = 0.4g used in designing the 20-storey benchmark structure building [34]. It is therefore expected that the structure will behave nonlinearly (i.e., some plastic hinges will form at the ends of beams and columns) under the considered seismic records. The time histories of the chosen records are plotted in Fig. 11.

D. PERFORMANCE CRITERIA

In order to assess the performance of the proposed metaheuristic optimal FLC design approach, different performance criteria (PCs) are utilized for the actively controlled benchmark 20-storey structure. Following common practices [34], performance of the control system is gauged

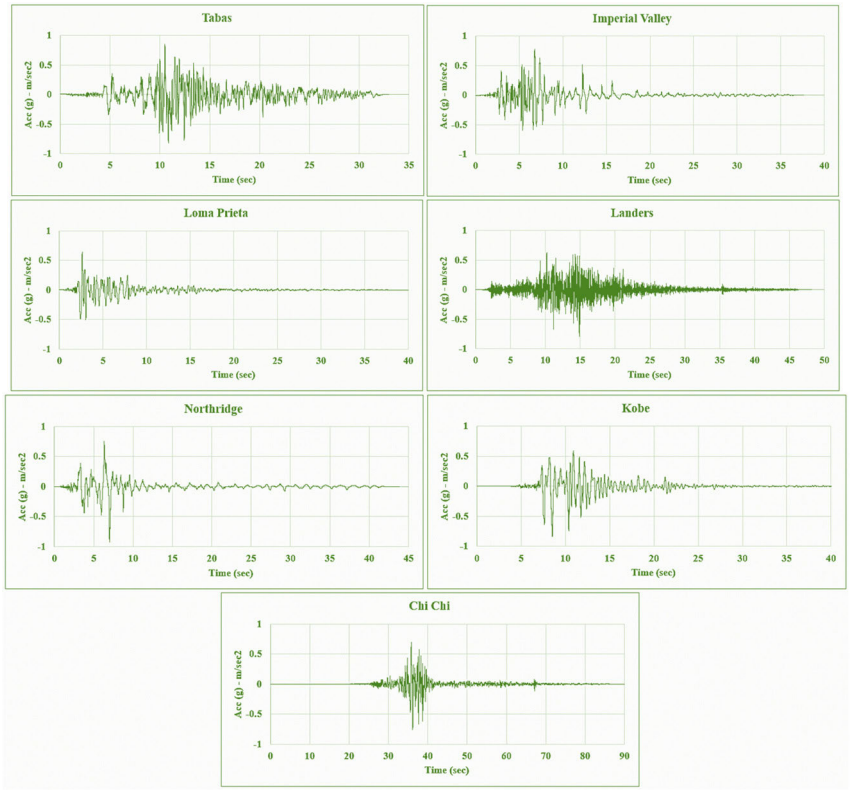

FIGURE 11. Acceleration time histories of the recorded seismic ground motion components in Table 4.

by comparing the response of the controlled structure to the response of the uncontrolled structure for the same earthquake excitation. In this regard, all PCs considered in this paper are ratios of some quantity of interest of the 20-storey MRF protected by the active control system with optimal FLC shown in Fig. 9 over the same or similar quantity for the 20-storey MRF with no control system shown in Fig. 8. Thus, lower PC values correspond to better performance of the active control system.

The adopted PCs are divided into three categories, examining maximum in time structural response, level of peak structural damage (i.e., material yielding), and maximum in time requirements of the control system. The first category of PCs includes the maximum inter-story drift ratio (i.e., relative peak displacement of two consecutive floors normalized by the floor height) of all stories, PC1, the maximum floor acceleration of all stories, PC2, and the maximum base shear (i.e., sum of horizontal structural forces resisting lateral sway), PC3, developed from all 7 ground motions (*EQs*) of Table 4. Mathematically, these PCs are expressed as

$$PC_1 = \max_{7EQs}\left\{\frac{\max\limits_{t,i}\frac{|d_i(t)|}{h_i}}{\delta^{max}}\right\} \tag{8}$$

$$PC_2 = \max_{7EQs}\left\{\frac{\max\limits_{t,i}\ddot{x}_{ai}(t)\mid}{\ddot{x}_a{}^{max}}\right\} \tag{9}$$

$$PC_3 = \max_{7EQs}\left\{\frac{\max\limits_{t,i}\left|\sum_i m_i\ddot{x}_{ai}(t)\right|}{F_b^{max}}\right\} \tag{10}$$

where, $d_i\,(t)$ is the time-history of the inter-story drift ratio of the ith storey of the controlled structure, h_i is the ith storey height, δ^{max} is the peak inter-story drift ratio from all the stories of the uncontrolled structure, $\ddot{x}_{ai}\,(t)$ is the acceleration time-history of the ith floor of the controlled structure, $\ddot{x}_a^{max}$ is the peak floor acceleration from all the floors of the uncontrolled structure, m_i is the seismic mass of the ith floor and F_b^{max} is the peak base shear of the uncontrolled structure.

The second category of PCs looks at the maximum ductility ratio (i.e., ratio of peak inelastic deformation over yielding deformation), PC4, the maximum seismic energy dissipation at plastic hinges, PC5, and the number of plastic hinges, PC6. In the definition of PC4 and PC5, the sum of the maximum curvature (i.e., second derivative of the deflection) at both ends of structural members are considered. The mathematical expressions of PCs quantifying structural damage level are given as

$$PC_4 = \max_{7EQs}\left\{\frac{\max\limits_{t,j}\frac{|\varphi_j(t)|}{\varphi_{yj}}}{\varphi_{max}}\right\} \tag{11}$$

$$PC_5 = \max_{7EQs}\left\{\frac{\max\limits_{t,j}\frac{\int dE_j}{M_{yj}\cdot\varphi_{yj}}}{E^{max}}\right\} \tag{12}$$

$$PC_6 = \max_{7EQs}\left\{\frac{N_d^c}{N_d}\right\} \tag{13}$$

where $\varphi_j(t)$ is the time-history of the curvature at the ends of the jth structural element in the controlled structure, φ_{yj} is the yield curvature at the ends of the jth structural element, φ^{max} is the maximum curvature over time across all the ends of structural members in the uncontrolled structure, $\int dE_j$ is the dissipated energy (i.e., area of the bending moment versus curvature graphs) at the ends of the jth structural member in controlled structure, M_{yj} is the yield moment at the ends of the jth structural element, E^{max} is the maximum energy dissipated over time across all the ends of structural members in the uncontrolled structure, and N_d^C and N_d are the numbers of plastic hinges (damaged ends of structural members) in the controlled and in the uncontrolled structure, respectively.

The third category of PCs includes the maximum control force, PC7, the maximum stroke of the actuators (i.e., relative displacement of the two device ends), PC8, and the maximum control power, PC9. The mathematical expressions of the last three PCs are given

$$PC_7 = \max_{7EQs}\left\{\frac{\max\limits_{t,k}|f_k(t)|}{W}\right\} \tag{14}$$

$$PC_8 = \max_{7EQs}\left\{\frac{\max\limits_{t,k}\left|y_k^a(t)\right|}{x^{max}}\right\} \tag{15}$$

$$PC_9 = \max_{7EQs}\left\{\frac{max\left|\sum P_l(t)\right|}{W\dot{x}^{max}}\right\} \tag{16}$$

where, f_k, y_k^a, and P_k are the time-histories of the control force, stroke, and required power of the kth actuator, respectively, W is the MRF total weight, and x^{max} and $\dot{x}^{max}$ are the maximum over time floor displacement and velocity relative to the ground of all floors of the uncontrolled structure.

V. STATEMENT OF THE FLC OPTIMIZATION PROBLEM

For the purposes of this work, the parametrically defined FLC in section II is optimized to minimize structural damage of the controlled benchmark structure due to the seismic records in Table 4. To this end, the peak ductility ratio in terms of sum of the curvature at the end of structural members is taken as a most representative quantity of the structural damage. This is closely related to PC4. However, for design purposes, PC4 is not used directly as the objective function to minimize as it does not account for the fact that records in Table 4 have different intensity and thus design would be dominated by the most severe record. Instead, a weighted sum approach is utilized in the definition of the objective function to minimize using the PGA of the records as weighting factors. This definition ensures that all records are accounted for in the FLC design independently of their intensity quantified by

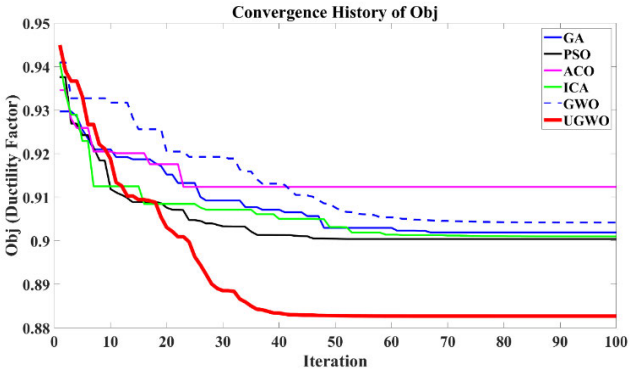

FIGURE 12. The convergence history of J objective function in Eq.(17) for the UGWO, GWO and four other metaheuristic optimization algorithms.

PGA. Mathematically, the objective function is written as

$$\mathrm{J} = \frac{\sum_{i=1}^{7}\left[PGA_i \times \max\limits_{\mathrm{i}}\left\{\frac{\max\limits_{t,j}\frac{|\varphi_j(t)|}{\varphi_{yj}}}{\varphi_{max}}\right\}\right]}{\sum_{i=1}^{7} PGA_i} \tag{17}$$

Thus, the FLC optimal design is formulated as follows: find the set of parameters defining the input fuzzification membership functions ($a_1, a_2, \ldots, a_{11}$, in Fig. 2) for each of the two input streams, the output defuzzification membership functions ($b_1, b_2, \ldots, b_{15}$, in Fig.2), and the fuzzy rule base ($c_1, c_2, \ldots, c_{64}$, in Table 2), for the four FLCs of the benchmark problem such that the objective function in Eq.(17) is minimized. In this regime, there are 101 design variables for each FLC, thus a total of 404 design variables are available.

VI. NUMERICAL APPLICATION

The fuzzy optimization problem detailed in the previous section is solved using the proposed UGWO, the standard GWO, as well as four other well-established in the literature metaheuristic optimization algorithms which have been used for FLC design applications as reviewed in the introduction, namely genetic algorithms (GA), particle swarm optimization (PSO), ant colony optimization (ACO), and imperialistic competitive algorithm (ICA). The same stopping criteria are applied for all the algorithms, that is, 3000 objective function evaluations and 100 iterations. The efficacy of the algorithms to reach a meritorious FLC design for seismic active control in tall buildings is gauged by utilizing the PCs of the benchmark problem detailed in section IV.

The convergence history of the objective function in Eq. (17) for the six different algorithms under testing are presented in Fig. 12. It is seen that the UGWO finds the best solution from all considered algorithms. Specifically, it achieves a value of $J = 0.8827$ for the objective function in Eq. (17), while the next best one is achieved by PSO ($J = 0.9004$), followed by ICA ($J = 0.9010$), GA ($J = 0.9019$), GWO ($J = 0.9042$), and ACO ($J = 0.9124$). It is also seen that the UGWO converges in fewer iterations from all other algorithms except for ACO, which however yields

TABLE 5. Optimized evaluation criteria for the 20-story building utilizing UGWO.

Performance criteria	Optimization algorithm	Earthquake ground motions						
		EQ1	EQ2	EQ3	EQ4	EQ5	EQ6	EQ7
PC1 drift ratio	UGWO	0.967	0.879	0.937	0.993	0.891	0.871	0.997
	GWO	0.969	0.925	0.963	**1.008**	0.899	0.934	**1.105**
	difference	0.23%	5.23%	2.72%	1.60%	0.90%	7.14%	10.89%
PC2 Story Acceleration	UGWO	0.938	0.953	0.945	0.936	**1.001**	0.937	0.975
	GWO	0.951	0.972	0.956	**1.029**	**1.006**	0.960	**1.034**
	difference	1.39%	1.92%	1.16%	9.88%	0.44%	2.50%	6.05%
PC3 Base Shear	UGWO	**1.045**	0.773	0.801	0.954	0.937	0.880	0.771
	GWO	0.985	0.818	0.779	0.958	0.937	0.890	0.793
	difference	**-5.70%**	5.81%	**-2.76%**	0.36%	0.03%	1.23%	2.79%
PC4 Ductility	UGWO	0.927	0.827	0.919	0.996	0.858	0.800	0.862
	GWO	0.934	0.830	0.963	**1.017**	0.860	0.858	0.884
	difference	0.68%	0.25%	4.77%	2.19%	0.27%	7.21%	2.61%
PC5 Dissipated Energy	UGWO	0.904	0.302	0.430	0.992	0.969	0.924	0.998
	GWO	**1.034**	0.457	0.518	**1.054**	**1.013**	0.975	**1.048**
	difference	14.38%	51.14%	20.40%	6.23%	4.52%	5.51%	4.93%
PC6 Plastic Hinges	UGWO	0.920	0.708	0.606	1.000	0.985	1.000	0.949
	GWO	0.960	0.792	0.636	**1.030**	**1.015**	**1.024**	0.974
	difference	4.35%	11.77%	5.00%	3.03%	3.09%	2.38%	2.71%
PC7 Control Force	UGWO	0.0071	0.0071	0.0070	0.0071	0.0071	0.0071	0.0070
	GWO	0.0074	0.0073	0.0074	0.0071	0.0074	0.0074	0.0073
	difference	4.23%	2.82%	5.71%	0.00%	4.23%	4.23%	4.29%
PC8 Device Stroke	UGWO	0.090	0.180	0.167	0.096	0.180	0.137	0.122
	GWO	0.091	0.187	0.171	0.098	0.181	0.146	0.125
	difference	0.22%	3.44%	2.76%	1.56%	0.89%	7.10%	2.37%
PC9 Control Power	UGWO	0.008	0.012	0.010	0.007	0.010	0.011	0.012
	GWO	0.009	0.013	0.011	0.004	0.009	0.009	0.013
	difference	3.57%	12.17%	6.93%	**-32.31%**	**-3.13%**	**-13.33%**	8.94%

the worst solution from all the considered algorithms and about 3.5% worse than the proposed UGWO. Through application of nonlinear time-domain analyses for the uncontrolled and the optimally FLC-based actively controlled benchmark structure, PCs in Eqs. (8-16) are derived for all the six metaheuristic optimization algorithms considered.

Table 5 reports PCs obtained for each of the 7 ground motions for the proposed UGWO and the standard GWO. It also reports the difference of the achieved PC values by the two algorithms with positive difference denoting improved performance of the proposed UGWO over the standard GWO. Besides the significant performance variability across different earthquake records, which is well-anticipated in structural earthquake engineering, it is seen that UGWO achieves better performance from the uncontrolled structure for all records for all PCs looking at peak structural responses (PC1-PC3) and level of inelastic response (PC4-PC6) indicative of structural damage, with only two exceptions highlighted in bold. Meanwhile, there are many more instances (13) for which the actively controlled structures using the standard GWO for FLC optimization performs worse than the uncontrolled structure. Moreover, with the exception of base shear PC3 for two records, the controlled structure with UGWO optimized FLC achieves improved performance than that of the GWO. The maximum improvements are up to 10.9% for PC1, 9.9% for PC2, 5.8% for PC3, 7.2% for PC4, 51.1% for PC5, and

TABLE 6. Maximum PC from seven earthquake records obtained by different metaheuristic algorithms and difference with respect to the proposed UGWO.

Performance criteria	Metaheuristic algorithms					
	GA	PSO	ACO	ICA	GWO	UGWO
PC1	1.046	1.064	1.045	1.039	1.105	0.997
difference	4.98%	6.80%	4.87%	4.29%	10.89%	-
PC2	1.018	1.010	1.014	1.019	1.034	1.001
difference	1.61%	0.89%	1.27%	1.80%	3.30%	-
PC3	1.050	1.039	1.046	1.044	0.985	1.045
difference	0.46%	**-0.52%**	0.15%	**-0.04%**	**-5.70%**	-
PC4	0.991	1.002	0.998	0.998	1.017	0.996
difference	**-0.48%**	0.69%	0.20%	0.21%	2.19%	-
PC5	1.033	1.069	1.058	1.076	1.054	0.998
difference	3.44%	7.07%	6.00%	7.74%	5.53%	-
PC6	1.061	1.030	1.030	1.031	1.030	1.000
difference	6.06%	3.03%	3.03%	3.05%	3.03%	-
PC7	0.0075	0.0073	0.0072	0.0078	0.0074	0.0071
difference	5.63%	2.82%	1.41%	9.86%	4.23%	-
PC8	0.198	0.197	0.200	0.198	0.187	0.180
difference	9.71%	9.04%	11.09%	9.93%	3.44%	-
PC9	0.008	0.013	0.008	0.008	0.013	0.012
difference	**-39.02%**	3.25%	**-37.40%**	**-36.59%**	8.94%	-

11.8% for PC6, which are quite significant. Importantly, these improvements by using reduced peak control forces and actuator strokes by up 4.3% and 7.1%, respectively. At the same time, higher peak control power is required for 3 out of the 7 records for UGWO to achieve the improved performances compared to GWO. Overall, the reported data suggest an overall considerable improvement in seismic structural performance in using the UGWO over the GWO for the optimal FLC design.

Further numerical data are provided in Table 6 to enable a comparison of the performance of the UGWO vis-à-vis all 5 alternative metaheuristic optimization algorithms considered in this work. Here, the peak PC value is reported from all seven records obtained by each algorithm together with percentage differences with respect to the UGWO. With very few exceptions concerning mostly the base shear related performance (PC3) which is most relevant to strength issues rather than seismically induced damage, the UGWO achieves better seismic performance of the controlled benchmark structure than the other metaheuristic algorithm. Improvements are in the range of 4.3% to 10.9% and 3% to 6% for the all-important drift ratio (PC1) and number of plastic hinges (PC6), respectively, achieved by exerting reduced peak control forces by 1.41% up to 9.86% and exhibiting reduced peak actuator stroke by 3.44% up to 11.1%. This data establishes the superiority of the proposed UGWO over several previously used metaheuristic algorithms for optimal FLC design in the rather challenging problem of seismic active control of tall buildings.

To gain further insights on the significance of the improved structural performance endowed by the UGWO over the GWO and over the uncontrolled structure, Figs. 13-15 present non-normalized data for the peak ductility ratio in terms of curvature and the peak energy dissipation ratio across all structural members of the benchmark structure, as well as the number of plastic hinges formed in the structure. Focusing first on the peak ductility ratio in Fig. 13, which is the most representative quantity of the level of highest damage in the structure, it is seen that the UGWO achieves always improvement compared to the uncontrolled structure, even in cases where the GWO does not improve the performance. The maximum difference of the UGWO and GWO in comparison to the uncontrolled structure are for the Kobe earthquake record of about 20% and 17%, respectively.

Next, the attention is turned to the seismic energy dissipation ratio in Fig.14 whose reduced value is good indicator of the potentially positive effect of active control to resist earthquake shaking with reduced structural damage and thus reduced repair costs and downtime after a major seismic event. It is found that for all earthquakes the controlled

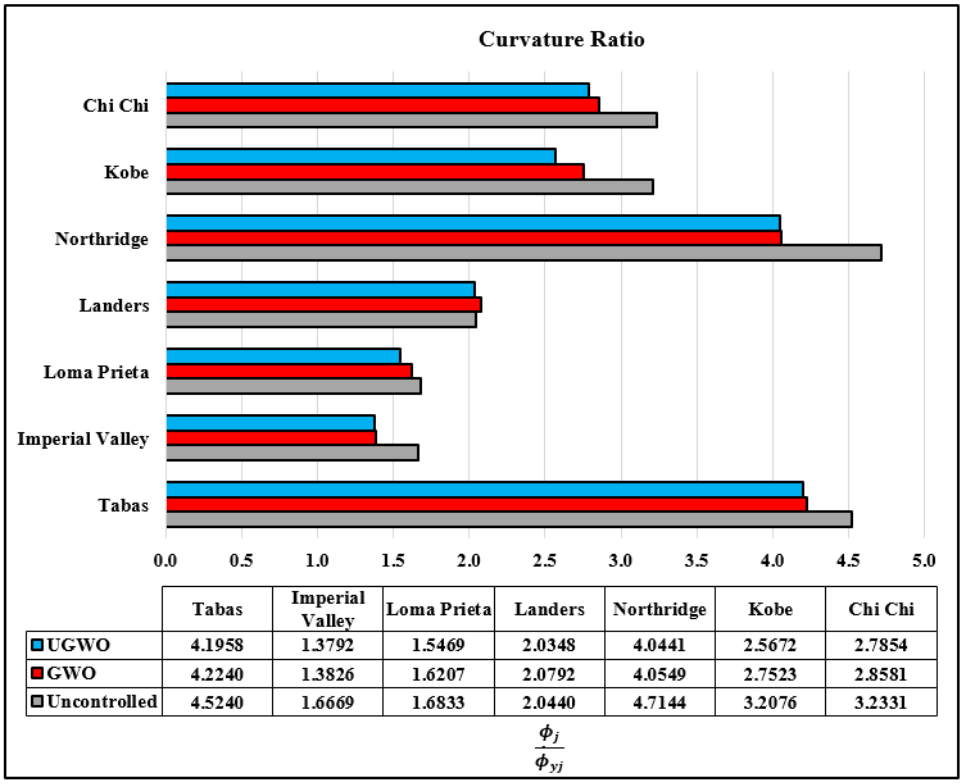

	Tabas	Imperial Valley	Loma Prieta	Landers	Northridge	Kobe	Chi Chi
UGWO	4.1958	1.3792	1.5469	2.0348	4.0441	2.5672	2.7854
GWO	4.2240	1.3826	1.6207	2.0792	4.0549	2.7523	2.8581
Uncontrolled	4.5240	1.6669	1.6833	2.0440	4.7144	3.2076	3.2331

FIGURE 13. Comparison of the curvature ratio for different earthquakes.

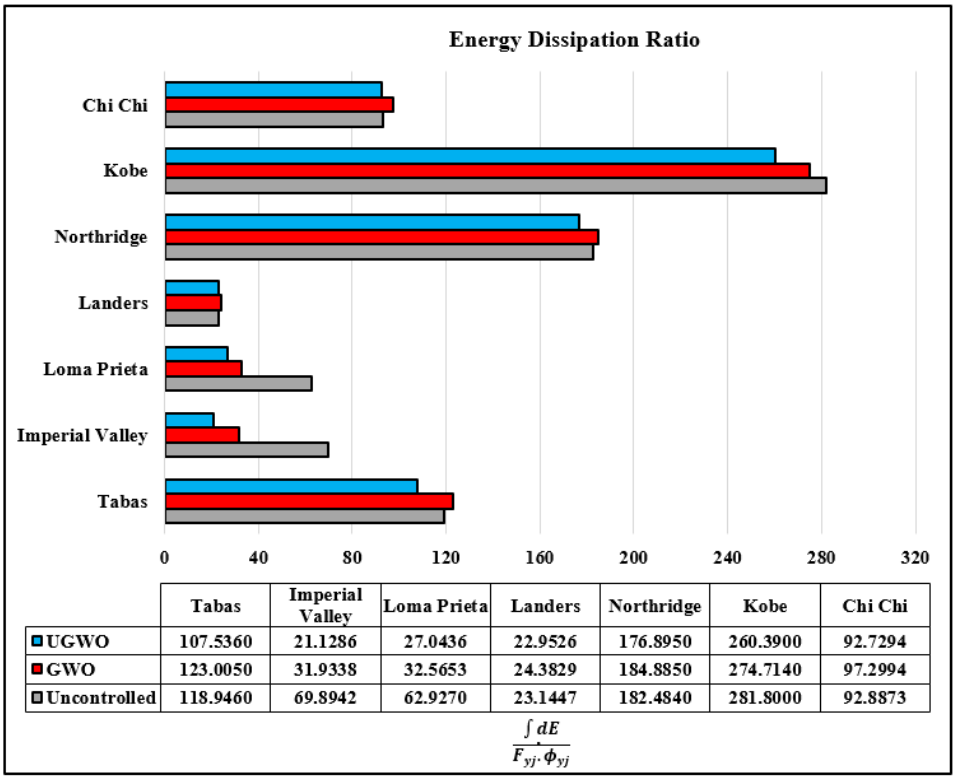

	Tabas	Imperial Valley	Loma Prieta	Landers	Northridge	Kobe	Chi Chi
UGWO	107.5360	21.1286	27.0436	22.9526	176.8950	260.3900	92.7294
GWO	123.0050	31.9338	32.5653	24.3829	184.8850	274.7140	97.2994
Uncontrolled	118.9460	69.8942	62.9270	23.1447	182.4840	281.8000	92.8873

FIGURE 14. Comparison of the energy dissipation ratio for different earthquakes.

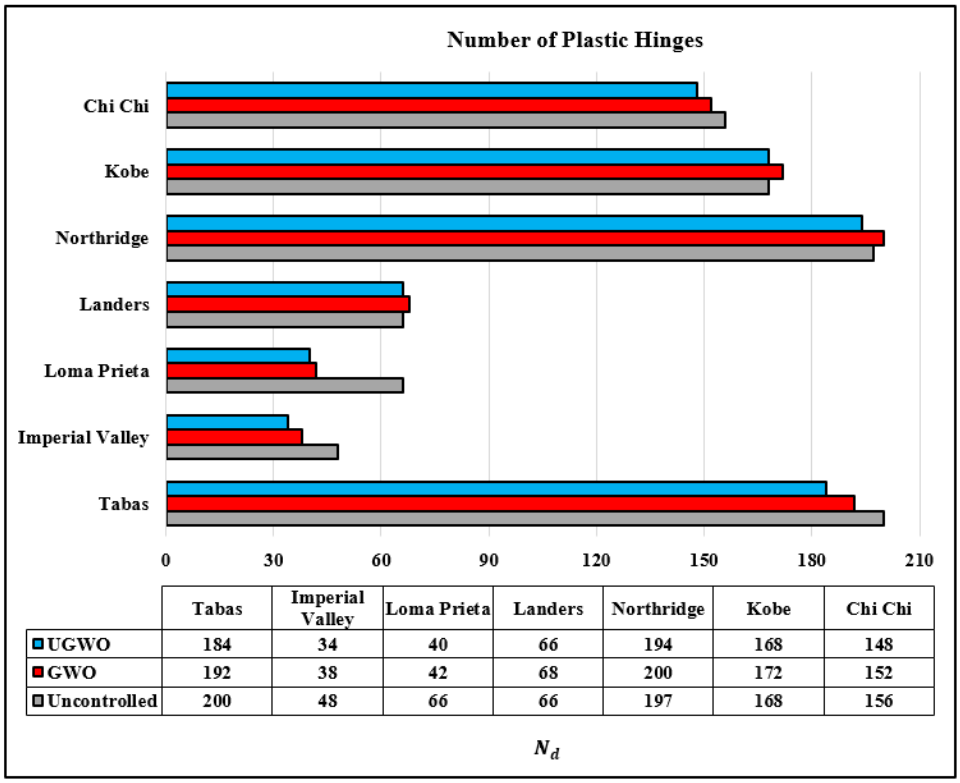

	Tabas	Imperial Valley	Loma Prieta	Landers	Northridge	Kobe	Chi Chi
UGWO	184	34	40	66	194	168	148
GWO	192	38	42	68	200	172	152
Uncontrolled	200	48	66	66	197	168	156

FIGURE 15. Comparison of the number of plastic hinges for different earthquakes.

benchmark structure optimized using the UGWO performs better from the uncontrolled, while this is not always the case with the GWO. Remarkably, for the imperial valley event, the UGWO achieves 70% reduced energy dissipation through plastic deformation compared to only 54% achieved by the GWO.

Lastly, looking at Fig. 15, similar observations can be made for the number of plastic hinges (i.e., locations of a local structural damage), for which the UGWO reduces the number of plastic hinges compared to the uncontrolled structures with the exception of Kobe and Landers seismic records for which the number of plastic hinges remain the same, though they slightly increase when using the GWO to optimize the FLC. Overall, despite record-to-record variability, the UGWO achieves always a better performance than GWO which establishes the superiority of the best agent updating within each iteration of the GWO algorithm proposed in this paper.

VII. CONCLUDING REMARKS

In this paper, an enhanced version of the GWO algorithm has been proposed for the optimal design of FLCs for seismic damage mitigation of tall buildings via active control. The efficacy of the upgraded algorithm, UGWO, has been demonstrated by considering a benchmark 20-storey steel frame building actively controlled using 25 actuators. To fulfill this aim, a fuzzy optimal design problem has been considered involving 404 design variables tuned to minimize the inelastic response of the actively controlled benchmark structure for 7 high-intensity near fault recorded ground motions. It was found that FLC optimization using the proposed UGWO achieves reduced seismic demands for most of the ground motions compared to the uncontrolled structure. The results have been compared to FLC-based actively controlled structure using GWO and four other metaheuristic optimization algorithms previously used in the literature as well. Seismic demands have been quantified in terms of six different performance indices including peak inter-storey drift, peak floor acceleration, peak ductility ratio, peak energy dissipation and number of plastic hinges developing. Further, the achieved higher reductions by the UGWO were accomplished using lower peak controlling force and peak actuator stroke. Overall, the reported numerical data establish the proposed UGWO as superior metaheuristic optimization algorithm for optimal FLC design and as a bona fide tool for reducing earthquake-induced damage to tall buildings under severe seismic events.

REFERENCES

[1] *MASNYC—The Municipal art Society of New York. The Accidental Skyline 2017. Report MASNYC 2017*. Accessed: Dec. 16, 2021. [Online]. Available: https://www.mas.org/news/the-accidental-skyline-2017/

[2] R. Bilham, "The seismic future of cities," *Bull. Earthq. Eng.*, vol. 7, no. 4, pp. 839–887, Nov. 2009.

[3] Z. Li and H. Adeli, "Control methodologies for vibration control of smart civil and mechanical structures," *Expert Syst.*, vol. 35, no. 6, Dec. 2018, Art. no. e12354.

[4] Y. K. Wen and M. Shinozuka, "Cost-effectiveness in active structural control," *Eng. Struct.*, vol. 20, no. 3, pp. 216–221, Mar. 1998.
[5] F. Freddi, C. Galasso, G. Cremen, A. Dall'Asta, S. L. Di, A. Giaralis, F. Gutiérrez-Urzúa, C. Málaga-Chuquitaype, S. A. Mitoulis, C. Petrone, and A. Sextos, "Innovations in earthquake risk reduction for resilience: Recent advances and challenges," *Int. J. Disaster Risk Reduction*, vol. 21, Apr. 2021, Art. no. 102267.
[6] R. M. Allen and D. Melgar, "Earthquake early warning: Advances, scientific challenges, and societal needs," *Annu. Rev. Earth Planet. Sci.*, vol. 47, no. 1, pp. 361–388, May 2019.
[7] K. Gkoktsi and A. Giaralis, "A compressive MUSIC spectral approach for identification of closely-spaced structural natural frequencies and post-earthquake damage detection," *Probabilistic Eng. Mech.*, vol. 60, Apr. 2020, Art. no. 103030.
[8] K. T. Tse, K. C. S. Kwok, and Y. Tamura, "Performance and cost evaluation of a smart tuned mass damper for suppressing wind-induced lateral-torsional motion of tall structures," *J. Struct. Eng.*, vol. 138, no. 4, pp. 514–525, Apr. 2012.
[9] F. Petrini, A. Giaralis, and Z. Wang, "Optimal tuned mass-damper-inerter (TMDI) design in wind-excited tall buildings for occupants' comfort serviceability performance and energy harvesting," *Eng. Struct.*, vol. 204, Feb. 2020, Art. no. 109904.
[10] L. Faravelli and T. Yao, "Use of adaptive networks in fuzzy control of civil structures," *Comput.-Aided Civil Infrastruct. Eng.*, vol. 11, no. 1, pp. 67–76, Jan. 1996.
[11] A. Tani, H. Kawamura, and R. Seiko, "Intelligent fuzzy optimal control of building structures," *Eng. Struct.*, vol. 20, no. 3, pp. 184–192, Mar. 1998.
[12] M. Al-Dawod, B. Samali, K. Kwok, and F. Naghdy, "Fuzzy controller for seismically excited nonlinear buildings," *J. Eng. Mech.*, vol. 130, no. 4, pp. 407–415, 2004.
[13] A. S. Ahlawat and A. Ramaswamy, "Multi-objective optimal design of FLC driven hybrid mass damper for seismically excited structures," *Earthq. Eng. Struct. Dyn.*, vol. 31, no. 7, pp. 1459–1479, 2002.
[14] A. S. Reddy, P. K. Agarwal, and S. Chand, "Adaptive multipopulation genetic algorithm based self designed fuzzy logic controller for active magnetic bearing application," *Int. J. Dyn. Control*, vol. 6, no. 3, pp. 1392–1408, Sep. 2018.
[15] D. Hein, S. Udluft, and T. A. Runkler, "Generating interpretable fuzzy controllers using particle swarm optimization and genetic programming," in *Proc. Genet. Evol. Comput. Conf. Companion*, Jul. 2018, pp. 1268–1275.
[16] J. Vanishree and V. Ramesh, "Optimization of size and cost of static VAR compensator using dragonfly algorithm for voltage profile improvement in power transmission systems," *Int. J. Renew. Energy Res.*, vol. 8, no. 1, pp. 56–66, Mar. 2018.
[17] R. Azizipanah-Abarghooee, M. Malekpour, M. Zare, and V. Terzija, "A new inertia emulator and fuzzy-based LFC to support inertial and governor responses using Jaya algorithm," in *Proc. IEEE Power Energy Soc. Gen. Meeting (PESGM)*, Jul. 2016, pp. 1–5.
[18] M. Hasanipanah, H. B. Amnieh, H. Khamesi, D. J. Armaghani, S. B. Golzar, and A. Shahnazar, "Prediction of an environmental issue of mine blasting: An imperialistic competitive algorithm-based fuzzy system," *Int. J. Environ. Sci. Technol.*, vol. 15, no. 3, pp. 551–560, Mar. 2018.
[19] H. Boubertakh, "Knowledge-based ant colony optimization method to design fuzzy proportional integral derivative controllers," *J. Comput. Syst. Sci. Int.*, vol. 56, no. 4, pp. 681–700, Jul. 2017.
[20] C. Caraveo, F. Valdez, and O. Castillo, "Optimization of fuzzy controller design using a new bee colony algorithm with fuzzy dynamic parameter adaptation," *Appl. Soft Comput.*, vol. 43, pp. 131–142, Jun. 2016.
[21] D. K. Sahoo, R. K. Sahu, G. T. C. Sekhar, and S. Panda, "A novel modified differential evolution algorithm optimized fuzzy proportional integral derivative controller for load frequency control with thyristor controlled series compensator," *J. Electr. Syst. Inf. Technol.*, vol. 5, no. 3, pp. 944–963, Dec. 2018.
[22] M. K. Debnath, J. R. Padhi, P. Satapathy, and R. K. Mallick, "Design of fuzzy-PID controller with derivative filter and its application using firefly algorithm to automatic generation control," in *Proc. 6th Int. Conf. Comput. Appl. Electr. Eng.-Recent Adv. (CERA)*, Oct. 2017, pp. 353–358.
[23] M. Gheisarnejad, "An effective hybrid harmony search and cuckoo optimization algorithm based fuzzy PID controller for load frequency control," *Appl. Soft Comput.*, vol. 65, pp. 121–138, Apr. 2018.
[24] B. P. Sahoo and S. Panda, "Improved grey wolf optimization technique for fuzzy aided PID controller design for power system frequency control," *Sustain. Energy, Grids Netw.*, vol. 16, pp. 278–299, Dec. 2018.
[25] M. M. Zadeh and S. M. T. Bathaee, "Load frequency control in interconnected power system by nonlinear term and uncertainty considerations by using of harmony search optimization algorithm and fuzzy-neural network," in *Proc. Iranian Conf. Electr. Eng. (ICEE)*, May 2018, pp. 1094–1100.
[26] F. Olivas, F. Valdez, P. Melin, A. Sombra, and O. Castillo, "Interval type-2 fuzzy logic for dynamic parameter adaptation in a modified gravitational search algorithm," *Inf. Sci.*, vol. 476, pp. 159–175, Feb. 2019.
[27] S. Talatahari, P. Motamedi, A. B. Farahmand, and M. Azizi, "Tribe–charged system search for parameter configuration of nonlinear systems with large search domains," *Eng. Optim.*, vol. 53, no. 1, pp. 18–31, Jan. 2021, doi: 10.1080/0305215X.2019.1696786.
[28] S. Talatahari and M. Azizi, "Optimal design of real-size building structures using quantum-behaved developed swarm optimizer," *Struct. Des. Tall Special Buildings*, vol. 29, no. 11, p. e1747, Aug. 2020, doi: 10.1002/tal.1747.
[29] S. Talatahari, M. Azizi, and M. Toloo, "Fuzzy adaptive charged system search for global optimization," *Appl. Soft Comput.*, vol. 24, May 2021, Art. no. 107518.
[30] S. Talatahari and M. Azizi, "Optimization of constrained mathematical and engineering design problems using chaos game optimization," *Comput. Ind. Eng.*, vol. 145, Jul. 2020, Art. no. 106560, doi: 10.1016/j.cie.2020.106560.
[31] M. Azizi, "Atomic orbital search: A novel metaheuristic algorithm," *Appl. Math. Model.*, vol. 93, pp. 657–683, May 2021, doi: 10.1016/j.apm.2020.12.021.
[32] M. Azizi, S. Talatahari, and A. Giaralis, "Optimization of engineering design problems using atomic orbital search algorithm," *IEEE Access*, vol. 9, pp. 102497–102519, 2021.
[33] S. Mirjalili, S. M. Mirjalili, and A. Lewis, "Grey wolf optimizer," *Adv. Eng. Softw.*, vol. 69, pp. 46–61, Mar. 2014.
[34] Y. Ohtori, R. E. Christenson, B. F. Spencer, Jr., and S. J. Dyke, "Benchmark control problems for seismically excited nonlinear buildings," *J. Eng. Mech.*, vol. 130, no. 4, pp. 366–385, Apr. 2004.
[35] A. Kaveh and S. Talatahari, "An enhanced charged system search for configuration optimization using the concept of fields of forces," *Struct. Multidisciplinary Optim.*, vol. 43, no. 3, pp. 339–351, 2011.
[36] I. Avramidis, A. Athanatopoulou, K. Morfidis, A. Sextos, and A. Giaralis, *Eurocode-Compliant Seismic Analysis and Design of R/C Buildings: Concepts, Commentary and Worked Examples With Flowcharts*. Cham, Switzerland: Springer, 2016, p. 488.
[37] N. M. Newmark, "A method of computation for structural dynamics," *J. Eng. Mech. Division*, vol. 85, no. 3, pp. 67–94, Jul. 1959.
[38] K. Subbaraj and M. A. Dokainish, "A survey of direct time-integration methods in computational structural dynamics—II. Implicit methods," *Comput. Struct.*, vol. 32, no. 6, pp. 1387–1401, Jan. 1989.
[39] Y. Ohtori and B. F. Spencer, Jr., "A MATLAB-based tool for nonlinear structural analysis," in *Proc. 13th Eng. Mech. Conf.*, Jun. 1999, pp. 13–16.
[40] K. Beyer and J. J. Bommer, "Selection and scaling of real accelerograms for bi-directional loading: A review of current practice and code provisions," *J. Earthq. Eng.*, vol. 11, no. S1, pp. 13–45, 2007.

MAHDI AZIZI received the Ph.D. degree in structural engineering from the University of Tabriz. He completed postdoctoral fellowship training in structural optimization with the University of Tabriz. He has published many research articles in the fields of structural optimization, metaheuristic algorithms, and structural vibration control, where his main purpose has been developing and hybridizing metaheuristic algorithms for different applications. He has recently proposed some novel metaheuristic algorithms for optimization purposes. He teaches some basic and advanced courses of structural engineering in different universities.

SIAMAK TALATAHARI received the Ph.D. degree in structural engineering. He joined the University of Tabriz (one of the top ten universities in Iran), where he is currently an Associate Professor. His research interests include data science (DS), machine learning (ML) and artificial intelligence (AI), and their application on engineering. Thanks to introduce, improve, hybridize and apply DS/AI/ML methods for engineering problems, he published over 120 refereed international journal articles, three edited books in Elsevier, eight chapters in international books. The citation of his works is over 8500. He has studied both how present novel efficient DS/AI/ML methods and how adaptive/improve the present methods to solve difficult problems. As instance, he presented Charged System Search, in 2010, Firefly Algorithm with Chaos, in 2013, Developed Swarm Optimizer, in 2016, Chaos Game Optimization, in 2020, Stochastic Paint Optimizer, in 2020, Crystal Structure Algorithm, in 2021, Material Generation Algorithm (MGA) as some new meta-heuristic algorithms. Multi Expression Programming, in 2014, Gene Expression Data Classification, in 2015, Linear Biogeography-based Programming, in 2018, are some other DS-based methods that are developed and applied by him for solving engineering problems. He is honored by many academic awards; he is recognized as ''Top One Percent Scientist of the World'' in the field of ''engineering'' and ''computer sciences'' for several years and as ''One of the 70 Most Influential Professors in The History of the Tabriz University.'' He was also recognized as ''Distinguished Scientist of Iranian Forefront of Sciences,'' ''Most Prominent Young Engineering Scientist,'' ''Distinguished Researcher,'' ''Top Young Researcher,'' ''Most Acclaimed Professor'' and ''Top Researcher and Teacher.'' In addition, he has been selected to receive the ''TWAS Young Affiliate-ship'' from the Central & South Asia Region and ''Elite Awards'' from Iranian Elites Organization. He served as the Lead or a Guest Editor of some special issue on different journals.

AGATHOKLIS GIARALIS received the M.Eng. (Greek Diploma) degree in structural engineering and the M.Sc. degree in earthquake resistant design of structures from the Department of Civil Engineering, Aristotle University of Thessaloniki, Greece, and the Ph.D. degree in civil engineering from Rice University, Houston, TX, USA, partly funded by a Fulbright Exchange Scholarship. He is currently a Senior Lecturer in structural engineering with the Department of Civil Engineering, City, University of London, where he works as the Director of the Research Centre for Civil Engineering Structures, leading the Smart Structures and Structural Health Monitoring Research Unit. He has coauthored more than 100 articles in peer-reviewed international journals and conference proceedings. His research interests include the areas of nonlinear stochastic dynamics, structural vibrations control, vibrations-based structural health monitoring, and earthquake engineering. Recent contributions include innovative lightweight structural vibration control device configurations enabling dynamic energy harvesting, optimal performance-based design methodologies for slender buildings equipped with motion control devices under wind and earthquakes excitations, and compressive data acquisition and processing techniques supporting low-power wireless sensors for health monitoring and assessment of civil engineering structures. He is also a Chartered Civil Engineer, a member of the American Society of Civil Engineers (ASCE), and a fellow of the Higher Educational Academy in U.K.